Molecular Therapy
Oncolytics
Original Article

Imaging CAR T-cell kinetics in solid tumors: Translational implications

Matthew S. Skovgard,[1] Hocine R. Hocine,[1] Jasmeen K. Saini,[1] Maxim Moroz,[2] Rebecca Y. Bellis,[1] Srijita Banerjee,[1] Aurore Morello,[1] Vladimir Ponomarev,[2] Jonathan Villena-Vargas,[1,3,5] and Prasad S. Adusumilli[1,4,5]

[1]Thoracic Service, Department of Surgery, Memorial Sloan Kettering Cancer Center, New York, NY 10065, USA; [2]Department of Radiology, Memorial Sloan Kettering Cancer Center, New York, NY 10065, USA; [3]Division of Thoracic Surgery, Department of Cardiothoracic Surgery, Weill Cornell Medicine-New York Presbyterian Hospital, New York, NY 10065, USA; [4]Center for Cell Engineering, Memorial Sloan Kettering Cancer Center, New York, NY 10065, USA

SUMMARY

Success in solid tumor chimeric antigen receptor (CAR) T-cell therapy requires overcoming several barriers, including lung sequestration, inefficient accumulation within the tumor, and target-antigen heterogeneity. Understanding CAR T-cell kinetics can assist in the interpretation of therapy response and limitations and thereby facilitate developing successful strategies to treat solid tumors. As T-cell therapy response varies across metastatic sites, the assessment of CAR T-cell kinetics by peripheral blood analysis or a single-site tumor biopsy is inadequate for interpretation of therapy response. The use of tumor imaging alone has also proven to be insufficient to interpret response to therapy. To address these limitations, we conducted dual tumor and T-cell imaging by use of a bioluminescent reporter and positron emission tomography in clinically relevant mouse models of pleural mesothelioma and non-small cell lung cancer. We observed that the mode of delivery of T cells (systemic versus regional), T-cell activation status (presence or absence of antigen-expressing tumor), and tumor-antigen expression heterogeneity influence T-cell kinetics. The observations from our study underscore the need to identify and develop a T-cell reporter—in addition to standard parameters of tumor imaging and antitumor efficacy—that can be used for repeat imaging without compromising the efficacy of CAR T cells *in vivo*.

INTRODUCTION

The efficacy of chimeric antigen receptor (CAR) T-cell therapy in solid tumors is limited by inefficient tumor T-cell infiltration and inadequate proliferation and accumulation of T cells, which are secondary to a lack of uniform and strong expression of antigen on cancer cells.[1,2] The infiltration of adoptively transferred T cells into solid tumors is currently assessed by analyzing biopsy specimens. However, as the performance of serial and multiple biopsies of metastatic sites is not feasible, the ability to interpret antitumor responses to immunotherapy is limited. Although flow cytometric-, immunohistochemical-, and polymerase chain reaction-based assays can detect the presence of CAR T cells in peripheral blood and tissue samples,[3] our understanding of CAR T-cell kinetics is limited by the lack of a dynamic imaging modality. To optimize the efficacy of CAR T-cell immunotherapy and gain insights into site-specific responses, it is critical to develop a noninvasive imaging modality that enables the monitoring of CAR T-cell trafficking in real time.

Immune checkpoint inhibitor agents are associated with improved survival in patients with solid tumors, which is achieved through the reactivation of T-cell responses.[4] In addition, immune checkpoint inhibitor agents have been shown to rescue exhausting CAR T cells and promote their functional persistence and antitumor efficacy.[5,6] A portion of patients receiving immunotherapy, both cell-based and checkpoint-blockade therapy, show responses on traditional imaging; however, in the majority of patients, noninvasive assessment of response to immunotherapy (by computed tomography [CT] and positron emission tomography [PET]) provides an inaccurate or incomplete picture, despite the use of several different assessment criteria, such as RECIST 1.1, mRECIST, and iRECIST.[7,8] Some patients experience initial "progression" of disease, as evidenced by increasing tumor volume or the appearance of new lesions on CT, followed by a favorable response to treatment.[9–11] This phenomenon, called "pseudoprogression," does not necessarily represent tumor cell growth but rather may reflect infiltrating immune cells and an appropriate inflammatory reaction. Similarly, some patients treated with induction immunotherapy experience tumor enlargement after therapy or the absence of visible regression on imaging; however, they demonstrate tumor cell death of up to 90% and extensive immune cell infiltration on pathological assessment.[12] A noninvasive imaging modality that can reliably detect and quantify immune cell infiltration in such cases would be beneficial.

An ideal noninvasive imaging method would facilitate the imaging of CAR T-cell trafficking, infiltration, and accumulation in intended and unintended organs following the administration of CAR T cells.

Received 11 November 2020; accepted 8 June 2021;
https://doi.org/10.1016/j.omto.2021.06.006.

[5]Senior author

Correspondence: Prasad S. Adusumilli, Thoracic Surgery, Department of Surgery, Memorial Sloan Kettering Cancer Center, New York, NY 10065, USA.
E-mail: adusumip@mskcc.org

Pulmonary sequestration and toxicity following systemic administration of nonspecifically activated T cells (activated as a result of the manufacturing process) or due to off-target recognition are areas of concern.[13] Regional administration of CAR T cells has been shown to promote antitumor efficacy against solid tumors within the pleural and peritoneal cavities and against intrahepatic and intracranial metastases.[6,14–21] Investigation of CAR T-cell kinetics following regional versus systemic administration can provide insights into the trafficking and accumulation of administered CAR T cells at tumor sites.

Tracking CAR T cells *in vivo* may be completed by directly or indirectly labeling CAR T cells. Direct labeling (e.g., ^{111}indium labeling, detectable by scintigraphy) comes with an inherent disadvantage, which is that detection over time is relatively short, as the signal produced is diluted as cells divide. Indirect labeling, which involves genetically engineering CAR T cells to express a reporter gene, may provide long-lasting detection. CAR T cells are tracked by administering the reporter gene's substrate, resulting in a signal detectable by optical imaging, PET-CT, or scintigraphy, depending on the reporter gene chosen. Several groups have investigated the use of immunoPET imaging,[22,23] and a first-in-human study demonstrated that clinical response on a per-lesion level correlated with the PET signal produced.[24] In this study, we use an optical luciferase-based reporter gene as it is highly sensitive in translational studies and can be serially imaged at relatively low cost. We also investigate the use of a PET-avid reporter, which provides three-dimensional (3D) organ-specific resolution.

In the present study, we investigated the imaging of adoptively transferred CAR T cells in well-characterized murine models of human mesothelioma and non-small cell lung cancer.[25,26] Using optimized protocols, we characterized CAR T-cell trafficking, infiltration, and accumulation in these solid tumor models with variable antigen expression after systemic versus regional administration of CAR T cells. By dual imaging of cancer and CAR T cells, we demonstrate the benefit in interpreting the antitumor response.

RESULTS

Standard curves of imaging with enhanced firefly luciferase (effLuc)-expressing CAR T cells and firefly luciferase (ffLuc)-expressing cancer cells *in vitro* and *in vivo*

We used a second-generation human mesothelin (MSLN)-specific CAR with a CD28/CD3ζ domain (M28z) with a retroviral vector (Figure 1A).[6,16] To facilitate imaging, M28z CAR T cells were cotransduced with an additional retroviral construct encoding effLuc,[27] which allows for the monitoring of CAR T cells by bioluminescence imaging (BLI). The transduction efficiency of T cells was confirmed by flow cytometric analysis of green fluorescent protein (GFP) expression for M28z and of Thy1.1 expression for effLuc (Figure 1B). M28z transduction efficiency across experiments varied between 45% and 60%, as indicated by GFP expression (Figure 1B, upper panel), and effLuc transduction varied between 10% and 30%, as indicated by Thy1.1 expression (Figure 1B, lower panel). EffLuc did not change MSLN-specific CAR T-cell cytolysis as measured by cytotoxicity assay (chromium release assay; Figure S1).

We next developed a standard curve for effLuc function *in vitro* and *in vivo* to determine the minimal and maximal T-cell dose for reliable signal and to accurately quantify the accumulation of T cells. For *in vitro* standardization, T-cell doses ranging from 2×10^4 to 6×10^5 were incubated with D-luciferin before imaging. The standard curve demonstrated a linear correlation between photon counts and effLuc-expressing CAR T cells (Figure 1C). For *in vivo* standardization, T-cell doses ranging from 1×10^5 to 1×10^6 were injected intrapleurally into nonobese diabetic (NOD)/severe combined immunodeficient (SCID)/γ_c^{null} (NSG) mice. Mice were imaged after CAR T-cell injection, and the standard curve again showed a positive linear correlation between the number of injected T cells and the signal intensity (photons per second) (Figure 1D).

To optimize tumor cell imaging, we used mesothelioma MSTO-211H cells retrovirally transduced to express the GFP/ffLuc fusion protein (MSTO G). Transduction was validated by flow cytometric analysis for GFP$^+$ cells. To generate antigen-positive cells expressing MSLN on the cell surface, MSTO G cells were transduced with the human MSLN variant 1 subcloned into an SFG retroviral vector (MSTO GM). GFP and MSLN expression were quantified by flow cytometric analysis (Figure 1E). *In vitro*, a linear positive correlation was observed between the number of MSTO GM tumor cells and the BLI signal (photons per second) (Figure 1F). We then performed *in vivo* standardization to confirm that ffLuc expression and the BLI signal accurately reflected the tumor burden in our pleural mesothelioma mouse model.[6,16,25] MSTO GM cells (1×10^3–1×10^6) were injected intrapleurally into NSG mice (Figure 1G). A positive linear correlation between the number of injected cells and the signal intensity was observed.

In vivo CAR T-cell kinetics in the presence or absence of tumor

Experiments were conducted to define the *in vivo* kinetics of adoptively transferred, systemically administered CAR T cells in the absence or presence of antigen-expressing tumors. We intravenously injected 1×10^6 M28z-effLuc CAR T cells into NSG mice without tumor. On serial imaging, peak signal intensity was detected in the lungs 4 h after CAR T-cell injection. The BLI signal intensity in the lungs gradually decreased up to 24 h, but T cells were sequestered in the lungs for up to 70 h (Figure 2A). At 14 h after administration, CAR T cells were observed to accumulate in the bone marrow, liver, spleen, and cervical lymph nodes. We then performed a second experiment, this time using mice in which flank tumor had been established with 1×10^6 antigen-expressing MSTO GM cells injected subcutaneously. At 14 days after the establishment of flank tumor, mice were treated with intravenous administration of 1×10^6 M28z CAR T cells. These mice had an initial accumulation of CAR T cells in the lungs on BLI (Figure 2B); signal intensity then decreased over a 24-h period, accompanied by an increase in the flank signal intensity by day 3 after CAR T-cell administration. By day 6, there was a noted increase in the signal intensity, reflecting the accumulation of M28z CAR T cells into the antigen-positive flank tumor. These results demonstrate CAR T-cell trafficking to the antigen-expressing tumor site after initial pulmonary sequestration as well as subsequent proliferation and accumulation at the tumor site, which is consistent with our

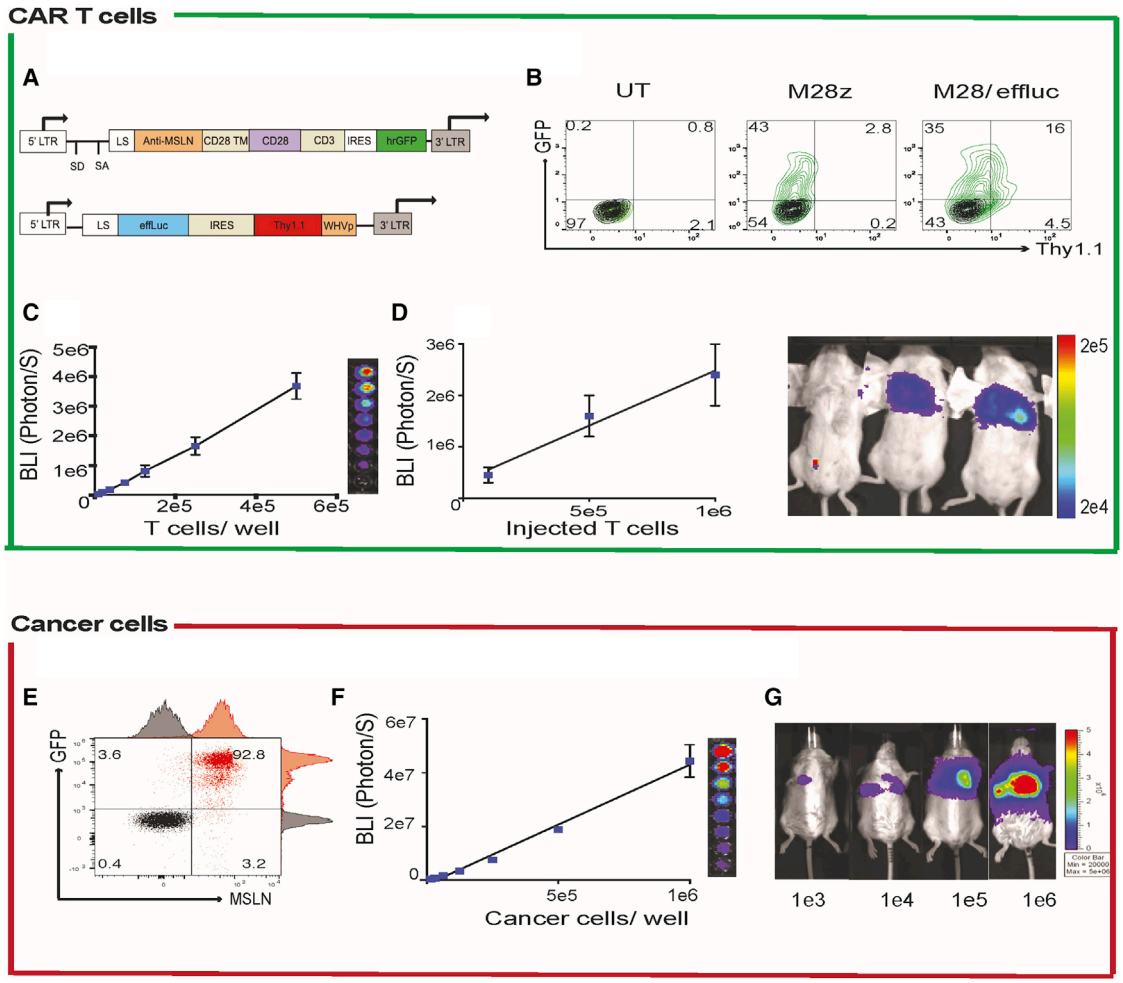

Figure 1. *In vitro* and *in vivo* standardization of CAR T-cell and cancer-cell imaging

(A) Construct map of second-generation MSLN-targeted construct with the CD28 co-stimulatory domain (M28z) and effLuc construct, with GFP and Thy1.1 as reporters. (B) Flow cytometric plots of untransduced (UT) and M28z (GFP^+), effLuc ($Thy1.1^+$), and dual-transduced M28z-effLuc (GFP^+, $Thy1.1^+$) T cells. (C) *In vitro* imaging standard curve of M28Z-effLuc CAR T cells (5×10^4–5×10^5) after addition of D-luciferin. (D) *In vivo* imaging standard curve of intrapleurally administered M28Z-effLuc CAR T cells (1×10^5, 5×10^5, and 1×10^6) after intraperitoneal injection of D-luciferin (n = 3 mice per dose). Images were taken using the Xenogen IVIS 100 imaging system. (E) Flow cytometric plots showing the transduction efficiency of luciferase (GFP^+) and MSLN ($MSLN^+$), compared with fluorescence-minus-one (black histogram). (F) *In vitro* imaging standard curve of mesothelioma cells with GFP with MSLN (MSTO GM) (1.5×10^4–2×10^6 cells). (G) *In vivo* imaging standard curve of intrapleurally injected MSTO GM cells (1×10^3, 1×10^4, 1×10^5, and 1×10^6) followed by intraperitoneal injection of D-luciferin (n = 2–3 mice per dose).

previously published results from immunohistochemical analysis of harvested organs.[6,16,28]

In vivo CAR T-cell kinetics in relation to the intensity of tumor-antigen expression

Having demonstrated that, at 72 h after treatment, CAR T cells accumulate within tumors expressing high levels of tumor antigen, we next questioned whether the density of antigen expression influences CAR T-cell kinetics, particularly given that human lung adenocarcinoma expresses MSLN heterogeneously.[25,26] To explore this, we used our model of lung adenocarcinoma,[26,29] which expresses MSLN at either high, low, or heterogenous levels (Figures 3A–3C). High-antigen-expressing tumors, composed of 1:1 A549GM and A549M cells, expressed MSLN in all cells, and 50% of cells were $ffLuc^+$ (A549GM), allowing for the regression of tumors with high-antigen-expressing cells to be assessed (Figure 3B). Imaging of tumors with low (1:1 A549G:A549E) or heterogenous (1:1 A549G:A549M) antigen expression specifically assesses the regression of low-antigen-expressing tumor cells in the presence of low- or high-antigen-expressing tumor cells (Figure 3B). Mice bearing tumors with low, heterogenous, or high antigen expression subsequently received a single low dose of CAR T cells (5×10^4) systemically. On tumor imaging (Figure 3C), regression of tumors with high antigen expression was evident, with tumor eradication at 8 days after CAR T-cell administration. Tumors with low antigen expression had delayed onset of tumor regression, which began 4 days after CAR T-cell administration. In an

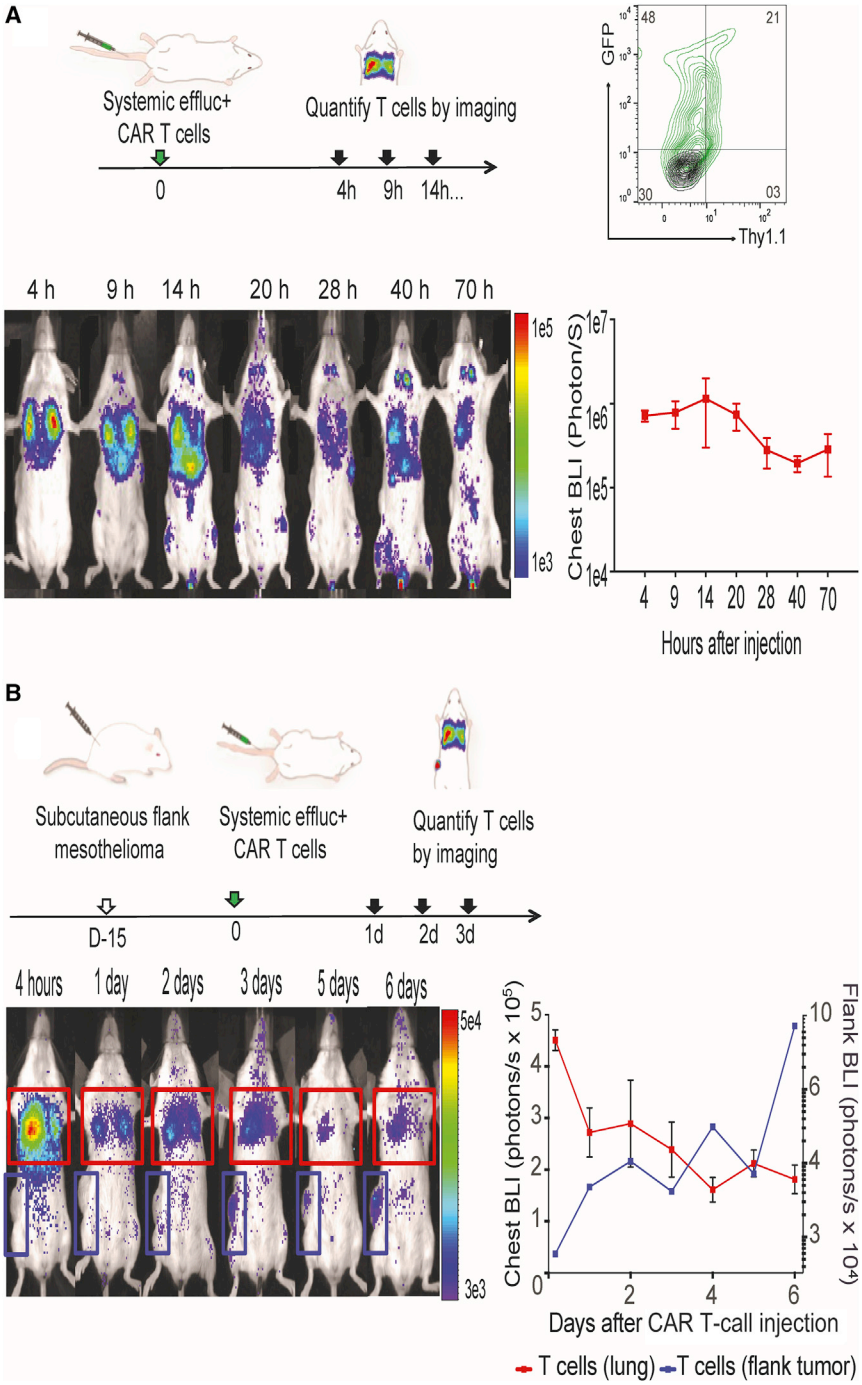

Figure 2. CAR T-cell imaging after systemic administration of T cells in mice with and without flank tumor

(A) Mice without tumor were administered M28z-effLuc CAR T cells (1×10^6), and T-cell kinetics were assessed by serial imaging for 70 h (n = 5 mice). Intravenously administered CAR T cells initially sequestered in the lung, with a maximum signal in the chest 4 h after injection and a steady decrease in fluorescence signal until 20 h after injection. (B) Mice (n = 3) with flank tumor established with 2×10^6 MSTO GM cells were treated with intravenous administration of 1×10^6 M28z-effLuc$^+$ CAR T cells. Quantitative BLI demonstrated a signal peak in the lung 4 h after injection (red solid line). Over a period of 24 h, decreased fluorescence was observed in the lung, with a concurrent increase in flank fluorescence signal, indicating CAR T-cell accumulation in the tumor. At day 6, the flank tumor fluorescence signal peaked, without a further decrease in lung signal, indicating proliferation of accumulated CAR T cells within the flank. Error bars represent ± standard error of the mean.

environment of heterogenous antigen expression, tumor cells with low antigen expression had early regression. Both low- and heterogenous antigen-expressing tumors eventually relapsed.

A separate experiment was designed to assess the imaging of CAR T cells in the above-mentioned mouse models with variable antigen expression (Figures 3D–3F). In mice that received non-MSLN-targeted control CAR T cells, T cells failed to accumulate at the tumor site (Figures 3F and 3G), resulting in tumor progression. In mice with tumors with high antigen expression—both tumors with homogeneous high antigen expression and tumors with heterogenous antigen expression—CAR T cells accumulated at the tumor site rapidly (Figures 3F and 3G. T-cell imaging (Figure 3F) and corollary tumor imaging (from the separate experiment of Figures 3A–3D) demonstrate that robust and early antitumor efficacy may correlate with CAR T-cell accumulation. Furthermore, as tumor with high antigen expression was eradicated, the CAR T-cell signal within the chest began to regress. In tumors with low antigen expression, CAR T-cell accumulation began early but progressed slowly. This slow accumulation was correlated with the observed delay in antitumor efficacy.

Regional administration of CAR T cells enhances early, robust CAR T-cell accumulation, which correlates with increased antitumor potency

Having demonstrated that CAR T-cell accumulation and potency depend on tumor-antigen density, we next postulated that the enhanced efficacy of regionally administered CAR T cells may be directly related to increased early accumulation of CAR T cells. Regionally delivered CAR T cells without antigenic stimulation (Figures 4A–4C) persisted in the pleural space for 5 days. There was no evidence, by T-cell imaging, of proliferation or egress, regardless of dose, until day 6 (Figure 4C). In mice with established antigen-positive orthotopic mesothelioma, a single dose of regionally delivered CAR T cells

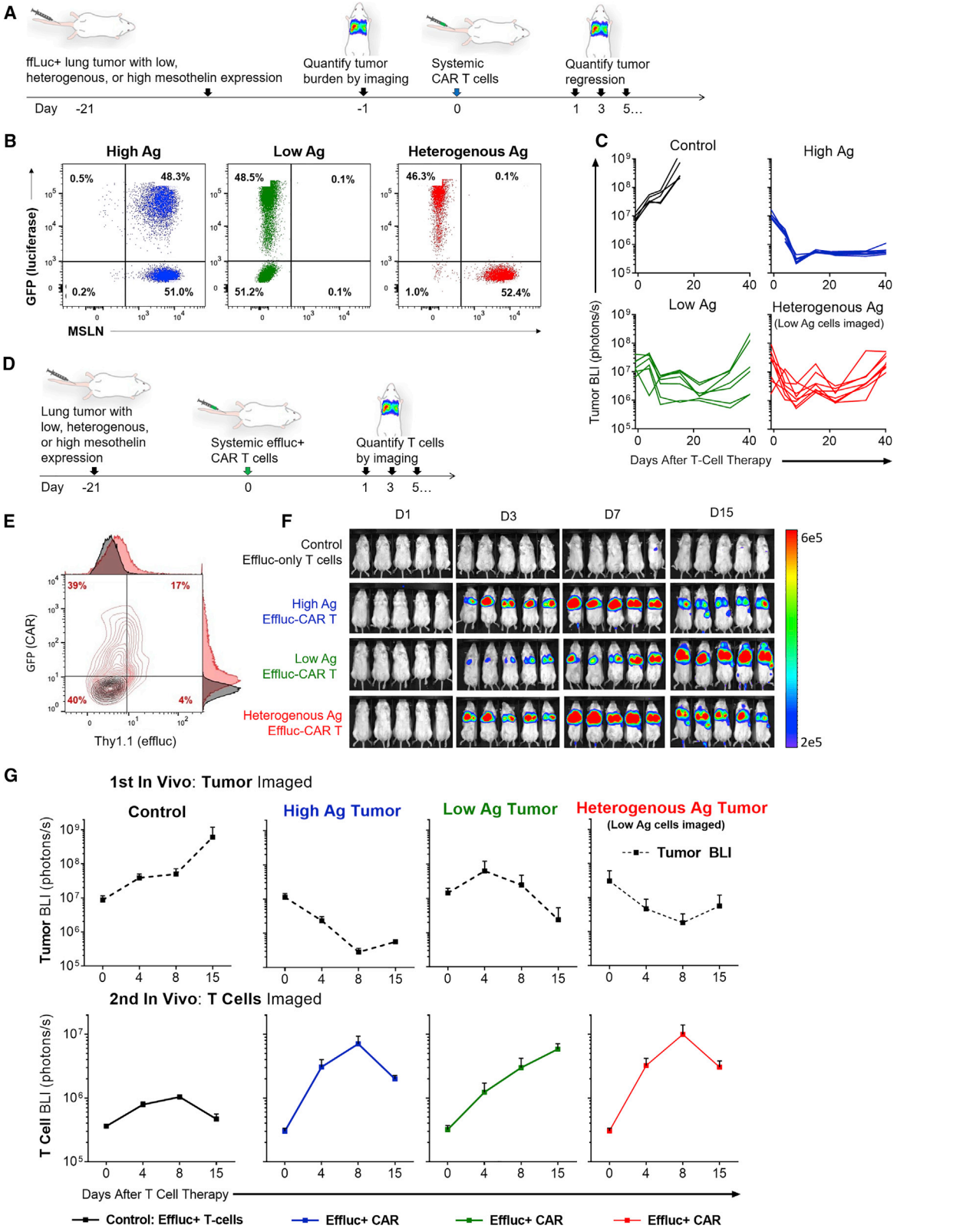

(legend on next page)

accumulated within the tumor and rapidly proliferated (Figures 4D and 4E). We observed a 6-fold increase in CAR T-cell imaging intensity 2 days after delivery (Figure 4F). In contrast, CAR T cells failed to accumulate in pleural tumors within 5 days after a single dose of systemically administered T cells. When T-cell imaging was compared with tumor imaging from a separate *in vivo* experiment (Figure 4F), CAR T-cell accumulation correlated with antitumor efficacy. Interestingly, as tumor was eradicated after regional delivery, CAR T cells continued to persist in the chest until at least 8 days after administration.

Dual imaging of CAR T cells and tumor by different imaging modalities

Given that concurrent imaging of tumor and T cells provided valuable insights into the clinical response to CAR T cells, we next investigated whether different reporter genes on T cells and tumor cells could be used to reliably assess antitumor efficacy. We cotransduced T cells with M28z CAR and *HSVtk* (herpes simplex virus thymidine kinase) (Figure 5A), a reporter gene that metabolizes a PET-CT-based reporter probe, ^{18}F-FEAU (2′-fluoro-2′-deoxy-1-β-D-arabinofuranosyl-5-ethyl-uracil). Mice with established ffLuc$^+$ orthotopic mesothelioma subsequently received regionally delivered HSVtk$^+$ M28z CAR T cells (Figure 5B). HSVtk$^+$ M28z CAR T-cell transduction efficiency was quantified by flow cytometry (Figure 5C). Reporter function was demonstrated by radiotracer uptake assay, and there was no difference in antigen-specific cytotoxicity *in vitro* as measured by chromium release assay (Figure S2B). Mice were subsequently imaged using bioluminescence imaging and PET-CT. Again, we observed that tumor regression (Figure 5D, left, BLI images) was correlated with CAR T-cell accumulation (Figure 5D, right, PET images). Furthermore, PET-CT allows for analysis and 3D characterization of organ-specific CAR T-cell accumulation.

DISCUSSION

The kinetics of pharmacotherapeutic agents play an important role in determining dose, assessing toxicity, and developing regimens in combination with other agents. CAR T cells are "living drugs," as the dose expands within the body, traffics differentially to multiple organ sites, accumulates in tumors depending on the intensity of antigen expression, and remains in the body for a long duration.[6,16,28,30,31] Furthermore, unlike chemical agents, whose serum concentration can be used as a biomarker to predict efficacy and toxicity, solid tumor CAR T-cell therapy has no such marker available. Whereas chemical agents are manufactured and delivered uniformly to all patients, autologous CAR T cells are manufactured for each individual patient, with variable phenotype and transduction percentages.[32–34] Furthermore, it is not feasible to predict secondary expansion and recirculation of CAR T cells after antigen-specific proliferation at different metastatic sites. Interpretation of CAR T-cell therapy response in solid tumors has been inconsistent, reflecting in part the lack of techniques to measure T-cell distribution and efficacy *in vivo*. Noninvasive imaging of CAR T-cell therapy using a reporter transgene is a useful method to address these limitations.[16,35–37]

In the present study, we used two different imaging techniques to efficiently quantify CAR T-cell kinetics and biodistribution: BLI and PET-CT. The reporters we investigated in this study are limited to use in preclinical models; our observations form a strong rationale to develop T-cell imaging markers that can be used in the clinic. Given the small size of T cells, their low metabolism compared with cancer cells, and the depth of human organs, the ideal translational reporter system will be able to generate a high signal intensity, will lack immunogenicity, and will have no effect on the efficacy of CAR T cells. Although *HSVtk* has been used in the imaging of biological agents, including oncolytic viruses,[38,39] our results demonstrate that HSVtk-M28z CAR T cells have less efficacy than M28z CAR T cells alone (Figure S2). Increasing the expression of HSVtk negatively affects the viability of CAR T cells, whereas decreasing the expression of HSVtk limits the sensitivity of T-cell detection by imaging.

In addition to the need to develop an ideal reporter system to image T cells, the imaging method needs to be validated in a clinically

Figure 3. Tumor and CAR T-cell imaging in a mouse model of high or low homogeneous and a mixture of high and low heterogenous antigen expressing lung cancer

(A and B) Tumor imaging: given that MSLN expression is heterogenous in lung adenocarcinoma, mice were established with lung adenocarcinoma tumors (1×10^6 ffLuc$^+$ A549 cells administered by tail vein) with high, low, or heterogenous (mixture of high and low) MSLN expression (n = 5–7 mice per group). Flow cytometric plots of cells with high (A549GM:A549M, 50:50), low (A549G:A549E, 50:50), or heterogenous (A549G:A549M, 50:50) MSLN expression are shown. (C) Mice were treated with 5×10^5 M28z CAR T cells, and therapy response was assessed using serial tumor BLI (n = 5–7 mice per group). Tumor imaging revealed rapid and complete regression of high-antigen-expressing tumor and delayed and incomplete regression of low-antigen-expressing tumor. Interestingly, imaging of heterogenous antigen-expressing tumor, which quantifies only low-antigen-expressing cells within the tumor, demonstrated rapid tumor regression followed by a period of stability and then relapse. (D and E) CAR T-cell imaging: in a further experiment, mice were established with lung adenocarcinoma tumor with high, low, or heterogenous (mixture of high and low) MSLN expression and were treated with systemic administration of effLuc$^+$ CAR T cells (n = 5 mice per group). T-cell accumulation was quantified by T-cell imaging. (F) Control CAR T cells failed to accumulate within the tumor. MSLN-targeted CAR T cells displayed early and increasing accumulation in high-antigen-expressing and heterogenous antigen-expressing tumors, whereas accumulation was delayed in low-antigen-expressing tumors. (G) Quantitative imaging from separate experiments of (1) tumor and (2) CAR T cells. Average tumor BLI from experimentation in (A) demonstrates tumor progression in control mice. In mice receiving CAR T cells, there was brisk and large regression of high-antigen-expressing tumor, delayed and less regression of low-antigen-expressing tumor, and brisk, but less regression of low-antigen cells in a heterogenous-antigen-expressing tumor. In a second experiment (from D), by average CAR T-cell BLI, CAR T-cell kinetics correspond with tumor regression. Control mice fail to accumulate T cells within the chest, high-antigen-expressing and heterogenous antigen-expressing tumors rapidly accumulate CAR T cells, and in low-antigen-expressing tumors, CAR T cells begin accumulation early, but accumulation kinetics were slow, corresponding with delayed and inadequate tumor regression. Error bars represent ± standard error of the mean. Ag, antigen.

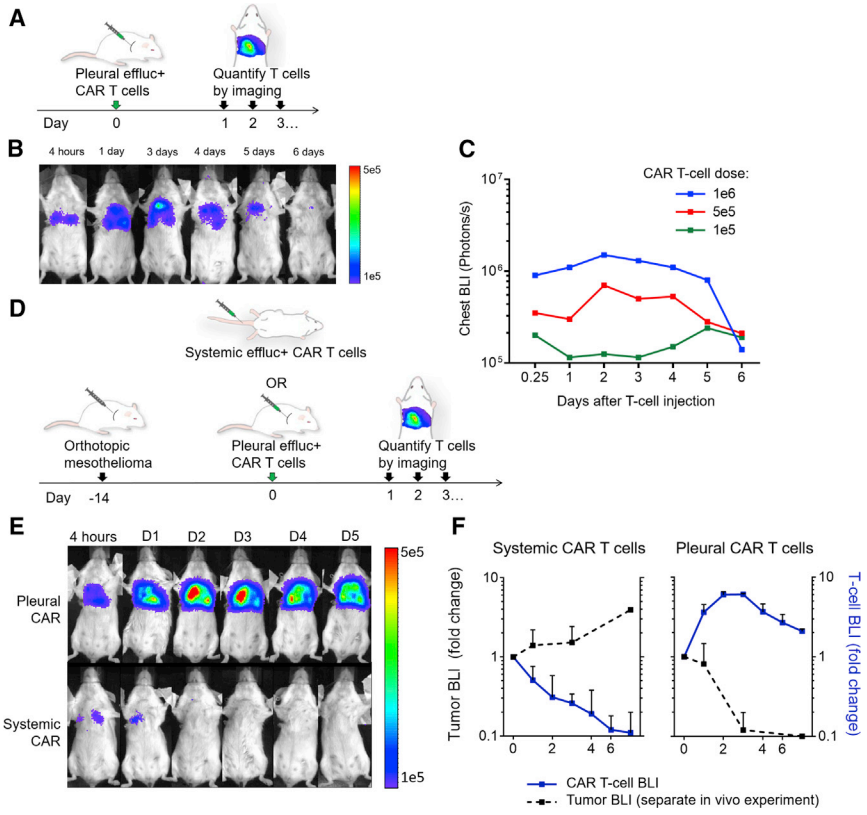

Figure 4. Regional administration of CAR T cells results in early, robust proliferation and antitumor efficacy

(A) EffLuc$^+$ CAR T cells were administered regionally by intrapleural injection at varying doses (5×10^5, 5×10^5, and 1×10^6, n = 3 mice per dose). (B and C) T-cell imaging showed that CAR T cells persisted within the pleural space for up to 5 days in the absence of pleural tumor. (D) Mice were established with orthotopic mesothelioma, followed by treatment with a single low dose of effLuc$^+$ intrapleural or systemic CAR T cells (n = 5 mice per group). (E) Intrapleurally administered T cells proliferated within the pleural cavity, whereas systemically administered CAR T cells failed to accumulate in the tumor. (F) T-cell imaging (in blue, n = 5 mice per group) from (D) and (E) overlaid with tumor imaging from a second separate *in vivo* experiment (n = 7 mice per group). At a low dose, systemically administered CAR T cells failed to accumulate, and antitumor efficacy was not observed. In contrast, intrapleurally administered CAR T cells rapidly accumulated, and early, robust antitumor efficacy was observed. Error bars represent ± standard error of the mean.

relevant model.[25,40] The pleural mesothelioma mouse model we used in this study clinicopathologically and radiologically resembles malignant pleural mesothelioma in patients. Owing to the location of the pleural tumor (directly beneath the chest wall in both mice and patients), imaging sensitivity is high by both BLI and PET scan, even with a relatively small amount of T cells; in contrast, the depth of the nodule, especially when small, in solid organs such as the liver and lung may limit detection.[41–43] However, in the metastatic lung cancer model used in our study, owing to the diffuse nature of metastases established by tail vein injection, the sensitivity of T-cell imaging was high, enabling characterization of CAR T-cell kinetics.

It has been proposed that the kinetics of antigen-activated T cells and nonantigen-activated T cells may differ.[44,45] Our experiments, which were conducted in mice with and without tumor, demonstrate varied kinetics. Several mechanisms may underlie this variation, including upregulation of the T-cell chemokine receptor following antigen activation[44,46]; a tumor-induced chemokine gradient that promotes T-cell infiltration[47,48]; higher numbers of T cells following T-cell proliferation, with improved kinetics; and a migration gradient that is induced by activated CAR T-cell–secreted chemokines.[49,50] Systemically administered CAR T cells are sequestered in the lungs, as evidenced by a peak signal at 4 h that steadily decreased up to 24 h. The persistence of the signal within the lungs for 3 days is consistent with results from studies that used prostate-specific membrane antigen CAR T cells.[51,52] The presence of an antigen-expressing distant tumor did not promote higher exit of CAR T cells from the lungs. This observation prompts analysis of the kinetics of different phenotypes of cells from lungs to peripheral circulation. Nonspecific activation of CAR T cells resulting from manufacturing may contribute to pulmonary sequestration as well. As the protocols for manufacturing change, *in vivo* T-cell kinetics should be investigated to ensure that pulmonary sequestration is not prolonged, which, in addition to compromising efficacy, may also lead to untoward effects. Regionally administered CAR T cells, irrespective of tested doses, remain in the pleural cavity in the absence of tumor for at least 6 days without signal change followed by regression. In contrast, in the presence of antigen-expressing pleural tumors, signal intensity rapidly increases, possibly related to antigen-activated CAR T-cell proliferation. Signal intensity decreases following tumor regression, and there is a corresponding decrease in T-cell signal intensity with subsequent tumor eradication.

We have demonstrated that CAR T-cell accumulation is tumor antigen dependent. Tumors with high antigen expression exhibit robust early accumulation of CAR T cells, with rapid eradication of the tumor. In the setting of low antigen expression, however, CAR T cells accumulate relatively slowly (as observed on T-cell imaging), which accounts for the initial observation of tumor progression followed by slow tumor regression and eventual tumor relapse. However, in the presence of tumors with high antigen expression, CAR T cells do proliferate, with increasing signal intensity and subsequent tumor regression. These observations further highlight the need for timing of imaging and serial imaging—along with dual tumor and T-cell imaging—to accurately assess the kinetics of CAR T cells. One word of caution: we observed that the efficacy of CAR T cells is compromised with repeat imaging. It is advisable to investigate antitumor efficacy (tumor imaging for

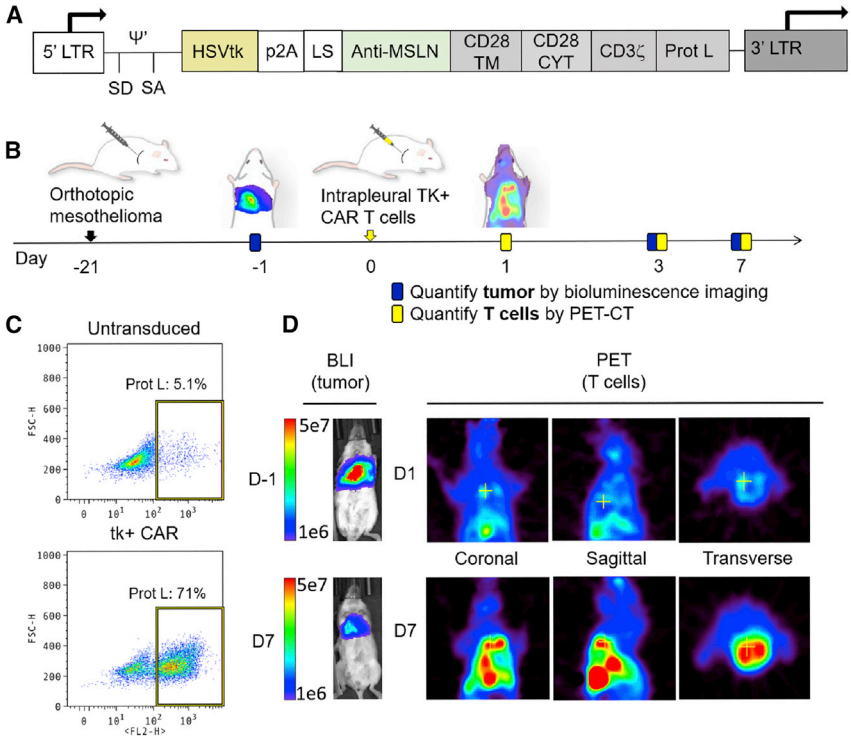

Figure 5. Thymidine kinase-positive CAR T-cell imaging with PET scan in parallel with tumor BLI

(A) *HSVtk* was cotransduced with our MSLN-targeted CAR. (B and C) Mice were established with ffLuc$^+$ orthotopic mesothelioma (n = 5 mice), and tumor burden was quantified using BLI. Mice were treated with a single dose of intrapleural HSVtk$^+$ CAR T cells, which can be quantified with micro-PET-CT via metabolism of the substrate ^{18}F-FEAU delivered intravenously. (D) Tumor BLI demonstrated antitumor efficacy, as evidenced by decreased tumor burden after increased intrapleural CAR T-cell accumulation by day 7 on T-cell PET scan. TK, thymidine kinase.

regression or progression and survival) and T-cell imaging for T-cell kinetics separately in 2 different experiments. In addition, to perform repeat T-cell imaging, the reporter system must have adequate sensitivity with minimal or no effect on T-cell efficacy, as T cells relative to tumor cells are small, few in number, and become exhausted.

Gaining early insight into which tumor sites may progress or relapse by tumor imaging and the accumulation of CAR T cells by the use of T-cell imaging are of critical importance in the era of clinical immuno-oncology. Solid tumors express antigen at varying densities within or between metastatic nodules.[2,26] This situation of variable expression is further complicated by the presence of unique tumor microenvironments, which may exhibit immunoinhibitory features.[53,54] The sensitivity of CT scan to detect treatment failure may be limited, particularly in the early phases of the treatment course.[55,56] We may therefore use T-cell imaging concurrently to quantify the immune kinetics at each tumor site and to characterize nodules earlier as either "immune-hot" or "immune-cold." The T-cell reporters used in preclinical models an in the clinic are highlighted in Table 1.

There are several limitations to our study. We used immunodeficient mouse models. While these models commonly used in preclinical studies of CAR T-cell therapy allow the investigation of human constructs and human T cells, for direct translation, a comprehensive tumor immune microenvironment is lacking. Immunosuppressive mechanisms derived from tumor-associated macrophages or myeloid-derived stem cells, for example, found in immunocompetent models play a key role in compromising the efficacy of adoptively transferred T cells, which may limit their proliferation, activation status, and kinetics. These mechanisms are not assessed in our study. Another limitation is the use of one type of CAR T-cell that targets MSLN. Further studies should be conducted to ensure that the kinetics we observe are applicable to CAR T cells with different antigen targets. Furthermore, owing to its optical nature and expected immunogenicity to a foreign protein, the luciferase reporter used in our system is not translatable to humans. Experiments using effLuc are also limited by the use of a single reporter to assess either tumor or T cells, as they cannot be quantified or localized simultaneously. This could be overcome by using a different reporter, as in experiments using *HSVtk*, but the impact on *in vivo* function must be assessed before translation. Transducing cells with *HSVtk* may result in compromised antitumor efficacy due to the untoward effects of *HSVtk* overexpression (Figure S2). Others[57–59] have identified candidate reporters with an acceptable immunotolerance profile that does not compromise antitumor efficacy (Table 1). However, optimization, translational studies, and clinical trials for many of these alternative reporter genes have not yet been performed.

In summary, our study underscores the importance of T-cell imaging, even in preclinical studies, to elucidate the differential kinetics related to tumor sites, T-cell activation status, mode of delivery, and heterogeneity of tumor-antigen expression. To advance adoptive T-cell therapy, it is critical to identify a T-cell reporter that can be detected on imaging even in deep, solid organs, that is not immunogenic, and that does not limit the antitumor efficacy of T cells.

MATERIALS AND METHODS

Tumor cells

MSTO-211H (human pleural mesothelioma) and A549 (human non-small cell lung cancer) cells were obtained from the American Type Culture Collection. To facilitate flow cytometric detection and noninvasive *in vivo* BLI, MSTO-211H and A549 cells were retrovirally transduced to express GFP-ffLuc$^+$. These cells were then transduced with the human MSLN variant 1 (isolated from the human ovarian cancer cell line OVCAR-3) subcloned into an SFG retroviral vector to generate MSTO MSLN+ GFP-ffLuc$^+$ or A549 MSLN+ GFP-ffLuc$^+$.

Table 1. T-cell imaging reporters used in preclinical models and in the clinic

Imaging modality	Reporter	Substrate	T cells identified in	Use in humans	Reference
Bioluminescence imaging	firefly luciferase	D-luciferin	mesothelioma, leukemia	–	16,60
	enhanced firefly luciferase	D-luciferin	mesothelioma, lymphoma	–	16,27
	Gaussia luciferase	coelenterazine	mesothelioma, lymphoma	–	16,36
	Renilla luciferase	coelenterazine	urothelial carcinoma, lymphoma	–	36,61
	click beetle red luciferase	D-luciferin	urothelial carcinoma	–	61
Positron emission tomography–computed tomography	*HSV-tk*	^{18}F-FHBG,^{124}I-FIAU, ^{18}F-FEAU	leukemia, lymphoma, mesothelioma, glioma	Yes	42,62–65
	human deoxycytidine kinase, hdCK3mut	^{18}F-FEAU ^{18}F-L-FMAU	prostate cancer, melanoma (M202 tumor)	–	66,67
	^{64}Cu-conjugated murine antibody	direct	lymphoma	–	68
	human norepinephrine transporter	^{18}F-MFBG, ^{124}I-MIBG	lymphoma	yes	69,70
	human somatostatin receptor type 2	68Ga-DOTATOC	anaplastic thyroid cancer	–	71
	^{89}Zr-anti-CD4 and -CD8 cys-diabodies	direct	stem cell transplantation	–	23
	^{89}ZR-oxine	direct	glioblastoma, prostate cancer	–	72
	^{18}F-AraG	direct	patients receiving radiation therapy or immunotherapy	yes	NCT03142204
	^{89}Zr-labeled pembrolizumab	direct	NSCLC, melanoma	yes	NCT03065764, NCT02760225
	prostate-specific membrane antigen	^{18}F-DCFPyL	leukemia	–	37
	^{89}Zr-labeled atezolizumab	direct	bladder cancer, NSCLC, breast cancer	yes	NCT02453984 NCT02478099[24]
Single-photon emission computed tomography or scintigraphy	human norepinephrine transporter	^{123}I-MIBG	EBV lymphoma, glioma	yes	69,70
	indium 111-oxine	direct	melanoma, colon, breast, and lung cancer	yes	NCT03853187[73–76]
	DOTA antibody reporter 1	86Y-AABD or 77Lu-AABD	leukemia	–	77

EBV, Epstein-Barr virus; NSCLC, non-small cell lung cancer.

Gammaretroviral vector construction and viral production

Construction and generation of the MSLN-specific CAR and control prostate-specific membrane antigen CAR have been described.[16] To facilitate the expression of a GFP reporter gene (*hrGFP*), bicistronic CARs were constructed by use of an internal ribosomal entry site (Figure 1A). The effLuc reporter gene was provided and described by P. Hwu (M.D. Anderson Cancer Center, Houston, TX).[27] Constructs were transfected into 293T H29 packaging cell lines, and viral supernatants were used to transduce and generate stable 293T RD114 cell lines.

Human T-cell transduction by CARs

T-cell transduction from healthy human volunteer donors (n = 5) under an institutional review board approval protocol with CAR was performed as previously described.[16] Two separate spinoculations were performed to transduce effLuc and M28z. Cells were maintained with 20 U/mL interleukin-2 (IL-2) (Life Technologies, Carlsbad, CA) administered every 48 h. Transduction efficiencies were determined by flow cytometry (as described below). Transduced cells were either used immediately in experiments or cultured in RPMI 1640 supplemented with 10% fetal bovine serum, 100 U/mL penicillin, 100 μg/mL streptomycin, and 20 U/mL interleukin-2. T-cell transduction efficiencies were determined by flow cytometric analysis (described below). Transduced cells were either used immediately in experiments or cultured in RPMI 1640 supplemented with 10% fetal bovine serum, 100 U/mL penicillin, 100 μg/mL streptomycin, and 20 U/mL IL-2.

Orthotopic pleural mesothelioma mouse model and intrapleural administration of CAR T cells

To develop the orthotopic mouse model of pleural mesothelioma, female NSG mice (Jackson Laboratory, Taconic, NY) at 6–10 weeks of

age were used. All of the procedures were performed under approved Institutional Animal Care and Use Committee protocols. Mice were anesthetized using inhaled isoflurane and oxygen and were administered bupivacaine for analgesia. Intrapleural injection of 1×10^6 tumor cells in 200 μL serum-free media via a right thoracic incision was performed to establish orthotopic malignant pleural mesothelioma tumors, as previously described.[25] In total, 5×10^4–2×10^6 transduced T cells were adoptively transferred into tumor-bearing mice 11–21 days after tumor injection; specifically, T cells were suspended in 200 μL serum-free media and were injected into the thoracic cavity of mice by direct pleural injection or systemically by tail vein injection. Assessment of tumor burden and T-cell trafficking was performed using BLI, as described below.

All of the mice were monitored every 15 min for the first hour following infusion of CAR T cells or tumor cells, and at least once daily for signs of toxicity. Humane endpoints included >20% body weight loss, change in physical appearance (e.g., ruffled hair), lethargy or persistent recumbency, loss of a righting reflex, or any condition interfering with daily activity. Once humane endpoints were reached, mice were sacrificed immediately. Mice were assessed for toxicity by trained animal workers, and they were blinded to the treatment groups to avoid subjective bias.

Non-small cell lung cancer mouse model and systemic administration of CAR T cells

To develop the mouse model of non-small cell lung cancer, female NSG mice at 6–10 weeks of age were used. All of the procedures were performed under approved Institutional Animal Care and Use Committee protocols, and mice were monitored as described above. Tumors with low antigen expression were established by the use of a mixture of 1:1 A549E (low MSLN) and A549G ($ffLuc^+$, low MSLN) cells. Tumors with heterogenous antigen expression were established by the use of a mixture of 1:1 $ffLuc^+$ A549G (low MSLN, $ffLuc^+$) and A549M ($MSLN^+$, ffLuc negative) cells. Tumors with high antigen expression were established by the use of a mixture of 1:1 A549GM ($ffLuc^+$, $MSLN^+$) and A549M cells. In total, 1×10^6 tumor cells in 200 μL serum-free media were injected via the dorsal tail vein. Twenty-one days after tumor cell inoculation, CAR T cells were administered as described above. Assessment of tumor burden and CAR T cells was performed using BLI, as described below.

Quantitative tumor and T-cell BLI

BLI was used *in vivo* to assess tumor burden in tumor-bearing mice. Animals were injected with a single intraperitoneal dose of 150 mg/kg D-luciferin. Mice were then imaged with the Xenogen IVIS 100 imaging system (Caliper Life Sciences, Boston, MA) 15 min after D-luciferin injection. Images were acquired for 5–30 s. BLI data were analyzed using Living Image software (version 4.31; Caliper Life Sciences); BLI signal is reported as total flux (photons per second). Individual mouse signals were determined by averaging the dorsal and ventral BLI signals for each animal using Microsoft Excel (Microsoft, Seattle, WA); the resulting data were analyzed using GraphPad Prism software (GraphPad Software, San Diego, CA). BLI was also used to visualize *in vivo* trafficking of adoptively transferred CAR T cells. T cells transduced with an effLuc reporter gene (provided by P. Hwu)[27] or *HSVtk* were transferred into mice by a single intrapleural or intravenous injection. These T cells could then be visualized by injecting the T-cell–bearing mice with a single intraperitoneal dose of 150 mg/kg D-luciferin and imaging the animals for 120 s at 20 min after injection, again using the Xenogen IVIS 100 imaging system.

PET imaging

For PET-CT imaging, mice were injected with 150 μCi ^{18}F-FEAU via the lateral tail vein. Sixty minutes after injection, PET and CT images were collected using a micro-PET-CT hybrid Inveon scanner (Siemens, Munich, Germany). Three-dimensional reconstructions were made using Inveon Research Workplace image analysis software (version 4.0; Siemens).

Radiotracer uptake assay

Cells were seeded in 15-cm culture plates at a density of 2×10^6 cells/mL and grown until 50% confluence. The incubation medium was replaced with 15 mL medium containing ^{3}H-FEAU (3.7 kBq/mL). The cells were harvested by scraping after periods of incubation (30, 60, and 120 min), and centrifuged at 1,250 × *g*. Cell pellets were weighed and reconstituted in solubilization buffer (Soluoene-350, PerkinElmer) and scintillation buffer (Insta-Fluor Plus; PerkinElmer). Using a TriCarb 1600 β-spectrometer (Packard), cell pellets were assayed for radioactivity concentration with standard ^{3}H-channel counting. Harvested cell-to-medium concentration ratios were determined and reported (dpm/g cells)/(dpm/mL medium). The radiochemical purity of each compound was checked by high-performance liquid chromatography to ensure >98% purity.

Flow cytometry

Expression of M28z and effLuc CAR was detected using GFP and Thy1.1 APC-conjugated $F(ab)_2$ anti-human immunoglobulin G1 (IgG1), respectively. Anti-human antibodies against CD3 (BD Biosciences, San Jose, CA) were used. Stained cells were processed using a FACScan instrument (BD Biosciences), and data were analyzed using FlowJo software (version 6.0; TreeStar, Ashland, OR).

SUPPLEMENTAL INFORMATION

Supplemental information can be found online at https://doi.org/10.1016/j.omto.2021.06.006.

ACKNOWLEDGMENTS

We thank Dr. Patrick Hwu of the M.D. Anderson Cancer Center (Houston, Texas) for providing the effLuc construct. We thank David B. Sewell of the Department of Surgery, Memorial Sloan Kettering Cancer Center, for excellent editorial assistance. The work of the P.S.A. laboratory is supported by grants from the National Institutes of Health (P30 CA008748, R01 CA236615-01, R01 CA235667, andT32CA009501), the US Department of Defense (BC132124, LC160212, CA170630, andCA180889), the Batishwa Fellowship, the Comedy vs Cancer Award, the Dalle Pezze Foundation, the Derfner

Foundation, the Esophageal Cancer Education Fund, the Geoffrey Beene Cancer Research Center, the Miner Fund for Mesothelioma Research, the Memorial Sloan Kettering Technology Development Fund, Mr. William H. Goodwin and Alice Goodwin, the Commonwealth Foundation for Cancer Research, the Experimental Therapeutics Center of Memorial Sloan Kettering Cancer Center, and ATARA Biotherapeutics. M.S.S. is supported in part by grant T32CA009501.

AUTHOR CONTRIBUTIONS

Conceptualization, P.S.A.; methodology, J.V.-V., V.P., A.M., and P.S.A.; validation, J.V.-V., A.M., V.P., and P.S.A.; investigation, J.V.-V., M.S.S., J.K.S., R.Y.B., M.M., V.P., A.M., and P.S.A.; formal analysis, J.V.-V., A.M., J.K.S., R.Y.B., M.S.S., H.R.H., M.M., V.P., and P.S.A.; writing – original draft, M.S.S., H.R.H., J.V.-V., and P.S.A.; writing – review & editing, all authors; visualization, J.K.S., R.Y.B., M.M., M.S.S., H.R.H., S.B., V.P., and P.S.A.; supervision, P.S.A.; funding acquisition, P.S.A.

DECLARATION OF INTERESTS

P.S.A. has received research funding from ATARA Biotherapeutics and Acea Biosciences; has served on the Scientific Advisory Board or as consultant to ATARA Biotherapeutics, Bayer, Carisma Therapeutics, Imugene, ImmPACT Bio, and Takeda Therapeutics; and has patents, royalties, and intellectual property on MSLN-targeted CARs and other T-cell therapies, which has been licensed to ATARA Biotherapeutics, as well as method for detection of cancer cells using virus, and pending patent applications on T-cell therapies. Memorial Sloan Kettering Cancer Center (MSK) has licensed intellectual property related to mesothelin-targeted CARs and T-cell therapies to ATARA Biotherapeutics, and has associated financial interests.

REFERENCES

1. Albelda, S.M. (2020). Tumor antigen heterogeneity: the "elephant in the room" of adoptive T-cell therapy for solid tumors. Cancer Immunol. Res. *8*, 2.
2. Morello, A., Sadelain, M., and Adusumilli, P.S. (2016). Mesothelin-targeted CARs: driving T cells to solid tumors. Cancer Discov. *6*, 133–146.
3. Hu, Y., and Huang, J. (2020). The chimeric antigen receptor detection toolkit. Front. Immunol. *11*, 1770.
4. Ribas, A., and Wolchok, J.D. (2018). Cancer immunotherapy using checkpoint blockade. Science *359*, 1350–1355.
5. Grosser, R., Cherkassky, L., Chintala, N., and Adusumilli, P.S. (2019). Combination immunotherapy with CAR T cells and checkpoint blockade for the treatment of solid tumors. Cancer Cell *36*, 471–482.
6. Cherkassky, L., Morello, A., Villena-Vargas, J., Feng, Y., Dimitrov, D.S., Jones, D.R., Sadelain, M., and Adusumilli, P.S. (2016). Human CAR T cells with cell-intrinsic PD-1 checkpoint blockade resist tumor-mediated inhibition. J. Clin. Invest. *126*, 3130–3144.
7. Seymour, L., Bogaerts, J., Perrone, A., Ford, R., Schwartz, L.H., Mandrekar, S., Lin, N.U., Litière, S., Dancey, J., Chen, A., et al.; RECIST working group (2017). iRECIST: guidelines for response criteria for use in trials testing immunotherapeutics. Lancet Oncol. *18*, e143–e152.
8. Schwartz, L.H., Litière, S., de Vries, E., Ford, R., Gwyther, S., Mandrekar, S., Shankar, L., Bogaerts, J., Chen, A., Dancey, J., et al. (2016). RECIST 1.1-update and clarification: from the RECIST committee. Eur. J. Cancer *62*, 132–137.
9. Wolchok, J.D., Hoos, A., O'Day, S., Weber, J.S., Hamid, O., Lebbé, C., Maio, M., Binder, M., Bohnsack, O., Nichol, G., et al. (2009). Guidelines for the evaluation of immune therapy activity in solid tumors: immune-related response criteria. Clin. Cancer Res. *15*, 7412–7420.
10. Gettinger, S.N., Horn, L., Gandhi, L., Spigel, D.R., Antonia, S.J., Rizvi, N.A., Powderly, J.D., Heist, R.S., Carvajal, R.D., Jackman, D.M., et al. (2015). Overall survival and long-term safety of nivolumab (anti-programmed death 1 antibody, BMS-936558, ONO-4538) in patients with previously treated advanced non-small-cell lung cancer. J. Clin. Oncol. *33*, 2004–2012.
11. Fujimoto, D., Yoshioka, H., Kataoka, Y., Morimoto, T., Hata, T., Kim, Y.H., Tomii, K., Ishida, T., Hirabayashi, M., Hara, S., et al. (2019). Pseudoprogression in previously treated patients with non–small cell lung cancer who received nivolumab monotherapy. J. Thorac. Oncol. *14*, 468–474.
12. Forde, P.M., Chaft, J.E., Smith, K.N., Anagnostou, V., Cottrell, T.R., Hellmann, M.D., Zahurak, M., Yang, S.C., Jones, D.R., Broderick, S., et al. (2018). Neoadjuvant PD-1 blockade in resectable lung cancer. N. Engl. J. Med. *378*, 1976–1986.
13. Morgan, R.A., Yang, J.C., Kitano, M., Dudley, M.E., Laurencot, C.M., and Rosenberg, S.A. (2010). Case report of a serious adverse event following the administration of T cells transduced with a chimeric antigen receptor recognizing ERBB2. Mol. Ther. *18*, 843–851.
14. Mulazzani, M., Fräßle, S.P., von Mücke-Heim, I., Langer, S., Zhou, X., Ishikawa-Ankerhold, H., Leube, J., Zhang, W., Dötsch, S., Svec, M., et al. (2019). Long-term in vivo microscopy of CAR T cell dynamics during eradication of CNS lymphoma in mice. Proc. Natl. Acad. Sci. USA *116*, 24275–24284.
15. Chekmasova, A.A., Rao, T.D., Nikhamin, Y., Park, K.J., Levine, D.A., Spriggs, D.R., and Brentjens, R.J. (2010). Successful eradication of established peritoneal ovarian tumors in SCID-Beige mice following adoptive transfer of T cells genetically targeted to the MUC16 antigen. Clin. Cancer Res. *16*, 3594–3606.
16. Adusumilli, P.S., Cherkassky, L., Villena-Vargas, J., Colovos, C., Servais, E., Plotkin, J., Jones, D.R., and Sadelain, M. (2014). Regional delivery of mesothelin-targeted CAR T cell therapy generates potent and long-lasting CD4-dependent tumor immunity. Sci. Transl. Med. *6*, 261ra151.
17. Katz, S.C., Burga, R.A., McCormack, E., Wang, L.J., Mooring, W., Point, G.R., Khare, P.D., Thorn, M., Ma, Q., Stainken, B.F., et al. (2015). Phase I hepatic immunotherapy for metastases study of intra-arterial chimeric antigen receptor-modified t-cell therapy for CEA+ liver metastases. Clin. Cancer Res. *21*, 3149–3159.
18. Adusumilli, P.S., Zauderer, M.G., Rusch, V.W., Cearbhaill, R.E., Zhu, A., Ngai, D.A., McGee, E., Chintala, N.K., Messinger, J.C., Vincent, A., et al. (2019). Abstract CT036. A phase I clinical trial of malignant pleural disease treated with regionally delivered autologous mesothelin-targeted CAR T cells: safety and efficacy. Cancer Res. *79*, CT036.
19. Adusumilli, P.S., Zauderer, M.G., Rusch, V.W., O'Cearbhaill, R., Zhu, A., Ngai, D., McGee, E., Chintala, N., Messinger, J., Cheema, W., et al. (2019). Regional delivery of mesothelin-targeted CAR T cells for pleural cancers: safety and preliminary efficacy in combination with anti-PD-1 agent. J. Clin. Oncol. *37*, 2511.
20. Priceman, S.J., Tilakawardane, D., Jeang, B., Aguilar, B., Murad, J.P., Park, A.K., Chang, W.-C., Ostberg, J.R., Neman, J., Jandial, R., et al. (2018). Regional delivery of chimeric antigen receptor-engineered T cells effectively targets $HER2^{+}$ breast cancer metastasis to the brain. Clin. Cancer Res. *24*, 95–105.
21. Murad, J.P., Kozlowska, A.K., Lee, H.J., Ramamurthy, M., Chang, W.-C., Yazaki, P., Colcher, D., Shively, J., Cristea, M., Forman, S.J., and Priceman, S.J. (2018). Effective targeting of $TAG72^{+}$ peritoneal ovarian tumors via regional delivery of CAR-engineered T cells. Front. Immunol. *9*, 2268.
22. England, C.G., Ehlerding, E.B., Hernandez, R., Rekoske, B.T., Graves, S.A., Sun, H., Liu, G., McNeel, D.G., Barnhart, T.E., and Cai, W. (2017). Preclinical pharmacokinetics and biodistribution studies of 89Zr-labeled pembrolizumab. J. Nucl. Med. *58*, 162–168.
23. Tavaré, R., McCracken, M.N., Zettlitz, K.A., Salazar, F.B., Olafsen, T., Witte, O.N., and Wu, A.M. (2015). Immuno-PET of murine T cell reconstitution postadoptive stem cell transplantation using anti-CD4 and anti-CD8 cys-diabodies. J. Nucl. Med. *56*, 1258–1264.
24. Bensch, F., van der Veen, E.L., Lub-de Hooge, M.N., Jorritsma-Smit, A., Boellaard, R., Kok, I.C., Oosting, S.F., Schröder, C.P., Hiltermann, T.J.N., van der Wekken, A.J., et al. (2018). ^{89}Zr-atezolizumab imaging as a non-invasive approach to assess clinical response to PD-L1 blockade in cancer. Nat. Med. *24*, 1852–1858.

25. Servais, E.L., Colovos, C., Rodriguez, L., Bograd, A.J., Nitadori, J., Sima, C., Rusch, V.W., Sadelain, M., and Adusumilli, P.S. (2012). Mesothelin overexpression promotes mesothelioma cell invasion and MMP-9 secretion in an orthotopic mouse model and in epithelioid pleural mesothelioma patients. Clin. Cancer Res. *18*, 2478–2489.

26. Kachala, S.S., Bograd, A.J., Villena-Vargas, J., Suzuki, K., Servais, E.L., Kadota, K., Chou, J., Sima, C.S., Vertes, E., Rusch, V.W., et al. (2014). Mesothelin overexpression is a marker of tumor aggressiveness and is associated with reduced recurrence-free and overall survival in early-stage lung adenocarcinoma. Clin. Cancer Res. *20*, 1020–1028.

27. Rabinovich, B.A., Ye, Y., Etto, T., Chen, J.Q., Levitsky, H.I., Overwijk, W.W., Cooper, L.J., Gelovani, J., and Hwu, P. (2008). Visualizing fewer than 10 mouse T cells with an enhanced firefly luciferase in immunocompetent mouse models of cancer. Proc. Natl. Acad. Sci. USA *105*, 14342–14346.

28. Kiesgen, S., Chicaybam, L., Chintala, N.K., and Adusumilli, P.S. (2018). Chimeric antigen receptor (CAR) T-cell therapy for thoracic malignancies. J. Thorac. Oncol. *13*, 16–26.

29. Servais, E.L., Colovos, C., Bograd, A.J., White, J., Sadelain, M., and Adusumilli, P.S. (2011). Animal models and molecular imaging tools to investigate lymph node metastases. J. Mol. Med. (Berl.) *89*, 753–769.

30. Savoldo, B., Ramos, C.A., Liu, E., Mims, M.P., Keating, M.J., Carrum, G., Kamble, R.T., Bollard, C.M., Gee, A.P., Mei, Z., et al. (2011). CD28 costimulation improves expansion and persistence of chimeric antigen receptor-modified T cells in lymphoma patients. J. Clin. Invest. *121*, 1822–1826.

31. Hocine, H.R., Quach, H.T., and Adusumilli, P.S. (2020). Commentary: long-term in vivo microscopy of CAR T cell dynamics during eradication of CNS lymphoma in mice. Front. Immunol. *11*, 1503.

32. Wang, X., and Rivière, I. (2016). Clinical manufacturing of CAR T cells: foundation of a promising therapy. Mol. Ther. Oncolytics *3*, 16015.

33. Sadelain, M., Brentjens, R., and Rivière, I. (2013). The basic principles of chimeric antigen receptor design. Cancer Discov. *3*, 388–398.

34. Wang, X., Naranjo, A., Brown, C.E., Bautista, C., Wong, C.W., Chang, W.-C., Aguilar, B., Ostberg, J.R., Riddell, S.R., Forman, S.J., and Jensen, M.C. (2012). Phenotypic and functional attributes of lentivirus-modified CD19-specific human CD8+ central memory T cells manufactured at clinical scale. J. Immunother. *35*, 689–701.

35. Emami-Shahri, N., Foster, J., Kashani, R., Gazinska, P., Cook, C., Sosabowski, J., Maher, J., and Papa, S. (2018). Clinically compliant spatial and temporal imaging of chimeric antigen receptor T-cells. Nat. Commun. *9*, 1081.

36. Santos, E.B., Yeh, R., Lee, J., Nikhamin, Y., Punzalan, B., Punzalan, B., La Perle, K., Larson, S.M., Sadelain, M., and Brentjens, R.J. (2009). Sensitive in vivo imaging of T cells using a membrane-bound Gaussia princeps luciferase. Nat. Med. *15*, 338–344.

37. Minn, I., Huss, D.J., Ahn, H.H., Chinn, T.M., Park, A., Jones, J., Brummet, M., Rowe, S.P., Sysa-Shah, P., Du, Y., et al. (2019). Imaging CAR T cell therapy with PSMA-targeted positron emission tomography. Sci. Adv. *5*, eaaw5096.

38. Haddad, D., and Fong, Y. (2015). Molecular imaging of oncolytic viral therapy. Mol. Ther. Oncolytics *1*, 14007.

39. Gil, Z., Kelly, K.J., Brader, P., Shah, J.P., Fong, Y., and Wong, R.J. (2008). Utility of a herpes oncolytic virus for the detection of neural invasion by cancer. Neoplasia *10*, 347–353.

40. Walters, D.M., Stokes, J.B., Adair, S.J., Stelow, E.B., Borgman, C.A., Lowrey, B.T., Xin, W., Blais, E.M., Lee, J.K., Papin, J.A., et al. (2013). Clinical, molecular and genetic validation of a murine orthotopic xenograft model of pancreatic adenocarcinoma using fresh human specimens. PLoS ONE *8*, e77065.

41. Doubrovin, M., Serganova, I., Mayer-Kuckuk, P., Ponomarev, V., and Blasberg, R.G. (2004). Multimodality in vivo molecular-genetic imaging. Bioconjug. Chem. *15*, 1376–1388.

42. Koehne, G., Doubrovin, M., Doubrovina, E., Zanzonico, P., Gallardo, H.F., Ivanova, A., Balatoni, J., Teruya-Feldstein, J., Heller, G., May, C., et al. (2003). Serial in vivo imaging of the targeted migration of human HSV-TK-transduced antigen-specific lymphocytes. Nat. Biotechnol. *21*, 405–413.

43. Lee, J.T., Zhang, H., Moroz, M.A., Likar, Y., Shenker, L., Sumzin, N., Lobo, J., Zurita, J., Collins, J., van Dam, R.M., and Ponomarev, V. (2017). Comparative analysis of human nucleoside kinase-based reporter systems for PET imaging. Mol. Imaging Biol. *19*, 100–108.

44. Gasser, O., Missiou, A., Eken, C., and Hess, C. (2005). Human CD8+ T cells store CXCR1 in a distinct intracellular compartment and up-regulate it rapidly to the cell surface upon activation. Blood *106*, 3718–3724.

45. Brodovitch, A., Bongrand, P., and Pierres, A. (2013). T lymphocytes sense antigens within seconds and make a decision within one minute. J. Immunol. *191*, 2064–2071.

46. Mikucki, M.E., Fisher, D.T., Matsuzaki, J., Skitzki, J.J., Gaulin, N.B., Muhitch, J.B., Ku, A.W., Frelinger, J.G., Odunsi, K., Gajewski, T.F., et al. (2015). Non-redundant requirement for CXCR3 signalling during tumoricidal T-cell trafficking across tumour vascular checkpoints. Nat. Commun. *6*, 7458.

47. Uehara, J., Ohkuri, T., Kosaka, A., Ishibashi, K., Hirata, Y., Ohara, K., Nagato, T., Oikawa, K., Aoki, N., Harabuchi, Y., et al. (2017). Intratumoral injection of IFN-β induces chemokine production in melanoma and augments the therapeutic efficacy of anti-PD-L1 mAb. Biochem. Biophys. Res. Commun. *490*, 521–527.

48. Vilgelm, A.E., and Richmond, A. (2019). Chemokines modulate immune surveillance in tumorigenesis, metastasis, and response to immunotherapy. Front. Immunol. *10*, 333.

49. Galeano Niño, J.L., Pageon, S.V., Tay, S.S., Colakoglu, F., Kempe, D., Hywood, J., Mazalo, J.K., Cremasco, J., Govendir, M.A., Dagley, L.F., et al. (2020). Cytotoxic T cells swarm by homotypic chemokine signalling. eLife *9*, e56554.

50. Moser, B., Wolf, M., Walz, A., and Loetscher, P. (2004). Chemokines: multiple levels of leukocyte migration control. Trends Immunol. *25*, 75–84.

51. Lee, S.H., Soh, H., Chung, J.H., Cho, E.H., Lee, S.J., Ju, J.M., Sheen, J.H., Kim, H., Oh, S.J., Lee, S.J., et al. (2020). Feasibility of real-time in vivo 89Zr-DFO-labeled CAR T-cell trafficking using PET imaging. PLoS ONE *15*, e0223814.

52. Dobrenkov, K., Olszewska, M., Likar, Y., Shenker, L., Gunset, G., Cai, S., Pillarsetty, N., Hricak, H., Sadelain, M., and Ponomarev, V. (2008). Monitoring the efficacy of adoptively transferred prostate cancer-targeted human T lymphocytes with PET and bioluminescence imaging. J. Nucl. Med. *49*, 1162–1170.

53. Wang, P., Zhang, X., Sun, N., Zhao, Z., and He, J. (2020). Comprehensive analysis of the tumor microenvironment in cutaneous melanoma associated with immune infiltration. J. Cancer *11*, 3858–3870.

54. Kudo, Y., Haymaker, C., Zhang, J., Reuben, A., Duose, D.Y., Fujimoto, J., Roy-Chowdhuri, S., Solis Soto, L.M., Dejima, H., Parra, E.R., et al. (2019). Suppressed immune microenvironment and repertoire in brain metastases from patients with resected non-small-cell lung cancer. Ann. Oncol. *30*, 1521–1530.

55. Chaft, J.E., Dunphy, M., Naidoo, J., Travis, W.D., Hellmann, M., Woo, K., Downey, R., Rusch, V., Ginsberg, M.S., Azzoli, C.G., and Kris, M.G. (2016). Adaptive neoadjuvant chemotherapy guided by (18)F-FDG PET in resectable non-small cell lung cancers: the NEOSCAN trial. J. Thorac. Oncol. *11*, 537–544.

56. Dimou, A., Sherman, C., and Wrangle, J. (2016). Imaging in Advanced Non-Small Cell Lung Cancer: A Medical Oncology Perspective. J. Thorac. Imaging *31*, 238–242.

57. Krekorian, M., Fruhwirth, G.O., Srinivas, M., Figdor, C.G., Heskamp, S., Witney, T.H., and Aarntzen, E.H.J.G. (2019). Imaging of T-cells and their responses during anti-cancer immunotherapy. Theranostics *9*, 7924–7947.

58. Mezzanotte, L., van 't Root, M., Karatas, H., Goun, E.A., and Löwik, C.W.G.M. (2017). In vivo molecular bioluminescence imaging: new tools and applications. Trends Biotechnol. *35*, 640–652.

59. Moroz, M.A., Zhang, H., Lee, J., Moroz, E., Zurita, J., Shenker, L., Serganova, I., Blasberg, R., and Ponomarev, V. (2015). Comparative analysis of t cell imaging with human nuclear reporter genes. J. Nucl. Med. *56*, 1055–1060.

60. Knorr, D.A., Bock, A., Brentjens, R.J., and Kaufman, D.S. (2013). Engineered human embryonic stem cell-derived lymphocytes to study in vivo trafficking and immunotherapy. Stem Cells Dev. *22*, 1861–1869.

61. Kleinovink, J.W., Mezzanotte, L., Zambito, G., Fransen, M.F., Cruz, L.J., Verbeek, J.S., Chan, A., Ossendorp, F., and Löwik, C. (2019). A dual-color bioluminescence reporter mouse for simultaneous in vivo imaging of t cell localization and function. Front. Immunol. *9*, 3097.

62. Blasberg, R. (2002). PET imaging of gene expression. Eur. J. Cancer *38*, 2137–2146.

63. Hall, D.O., Hooper, C.E., Searle, J., Darby, M., White, P., Harvey, J.E., Braybrooke, J.P., Maskell, N.A., Masani, V., and Lyburn, I.D. (2018). 18F-Fluorodeoxyglucose

PET/CT and dynamic contrast-enhanced MRI as imaging biomarkers in malignant pleural mesothelioma. Nucl. Med. Commun. *39*, 161–170.

64. Yaghoubi, S.S., Jensen, M.C., Satyamurthy, N., Budhiraja, S., Paik, D., Czernin, J., and Gambhir, S.S. (2009). Noninvasive detection of therapeutic cytolytic T cells with 18F-FHBG PET in a patient with glioma. Nat. Clin. Pract. Oncol. *6*, 53–58.

65. Keu, K.V., Witney, T.H., Yaghoubi, S., Rosenberg, J., Kurien, A., Magnusson, R., Williams, J., Habte, F., Wagner, J.R., Forman, S., et al. (2017). Reporter gene imaging of targeted T cell immunotherapy in recurrent glioma. Sci. Transl. Med. *9*, eaag2196.

66. McCracken, M.N., Vatakis, D.N., Dixit, D., McLaughlin, J., Zack, J.A., and Witte, O.N. (2015). Noninvasive detection of tumor-infiltrating T cells by PET reporter imaging. J. Clin. Invest. *125*, 1815–1826.

67. Likar, Y., Zurita, J., Dobrenkov, K., Shenker, L., Cai, S., Neschadim, A., Medin, J.A., Sadelain, M., Hricak, H., and Ponomarev, V. (2010). A new pyrimidine-specific reporter gene: a mutated human deoxycytidine kinase suitable for PET during treatment with acycloguanosine-based cytotoxic drugs. J. Nucl. Med. *51*, 1395–1403.

68. Alam, I.S., Mayer, A.T., Sagiv-Barfi, I., Wang, K., Vermesh, O., Czerwinski, D.K., Johnson, E.M., James, M.L., Levy, R., and Gambhir, S.S. (2018). Imaging activated T cells predicts response to cancer vaccines. J. Clin. Invest. *128*, 2569–2580.

69. Doubrovin, M.M., Doubrovina, E.S., Zanzonico, P., Sadelain, M., Larson, S.M., and O'Reilly, R.J. (2007). In vivo imaging and quantitation of adoptively transferred human antigen-specific T cells transduced to express a human norepinephrine transporter gene. Cancer Res. *67*, 11959–11969.

70. Moroz, M.A., Serganova, I., Zanzonico, P., Ageyeva, L., Beresten, T., Dyomina, E., Burnazi, E., Finn, R.D., Doubrovin, M., and Blasberg, R.G. (2007). Imaging hNET reporter gene expression with 124I-MIBG. J. Nucl. Med. *48*, 827–836.

71. Vedvyas, Y., Shevlin, E., Zaman, M., Min, I.M., Amor-Coarasa, A., Park, S., Park, S., Kwon, K.-W., Smith, T., Luo, Y., et al. (2016). Longitudinal PET imaging demonstrates biphasic CAR T cell responses in survivors. JCI Insight *1*, e90064.

72. Bhatnagar, P., Li, Z., Choi, Y., Guo, J., Li, F., Lee, D.Y., Figliola, M., Huls, H., Lee, D.A., Zal, T., et al. (2013). Imaging of genetically engineered T cells by PET using gold nanoparticles complexed to Copper-64. Integr. Biol. *5*, 231–238.

73. Pittet, M.J., Grimm, J., Berger, C.R., Tamura, T., Wojtkiewicz, G., Nahrendorf, M., Romero, P., Swirski, F.K., and Weissleder, R. (2007). In vivo imaging of T cell delivery to tumors after adoptive transfer therapy. Proc. Natl. Acad. Sci. USA *104*, 12457–12461.

74. Bernhard, H., Neudorfer, J., Gebhard, K., Conrad, H., Hermann, C., Nährig, J., Fend, F., Weber, W., Busch, D.H., and Peschel, C. (2008). Adoptive transfer of autologous, HER2-specific, cytotoxic T lymphocytes for the treatment of HER2-overexpressing breast cancer. Cancer Immunol. Immunother. *57*, 271–280.

75. Grimfors, G., Schnell, P.O., Holm, G., Johansson, B., Mellstedt, H., Pihlstedt, P., and Björkholm, M. (1989). Tumour imaging of indium-111 oxine-labelled autologous lymphocytes as a staging method in Hodgkin's disease. Eur. J. Haematol. *42*, 276–283.

76. Fisher, B., Packard, B.S., Read, E.J., Carrasquillo, J.A., Carter, C.S., Topalian, S.L., Yang, J.C., Yolles, P., Larson, S.M., and Rosenberg, S.A. (1989). Tumor localization of adoptively transferred indium-111 labeled tumor infiltrating lymphocytes in patients with metastatic melanoma. J. Clin. Oncol. *7*, 250–261.

77. Krebs, S., Ahad, A., Carter, L.M., Eyquem, J., Brand, C., Bell, M., Ponomarev, V., Reiner, T., Meares, C.F., Gottschalk, S., et al. (2018). Antibody with infinite affinity for in vivo tracking of genetically engineered lymphocytes. J. Nucl. Med. *59*, 1894–1900.